# Reduced Expression *of Chl1* gene Impairs Insulin Secretion by Down-Regulating the Expression of Key Molecules of β-cell Function

**Authors**
Jalal Taneera[1], Sarah Dhaiban[1], Mahmood Hachim[1], Abdul Khader Mohammed[1], Debasmita Mukhopadhyay[1], Khuloud Bajbouj[1], Rifat Hamoudi[1, 2], Albert Salehi[3], Mawieh Hamad[1]

**Affiliations**
1  Sharjah Institute for Medical Research, University of Sharjah, Sharjah, United Arab Emirates
2  Division of Surgery and Interventional Science, University College London, London, UK
3  Department of Clinical Sciences, Division of Islets Cell Pathophysiology, Lund University, Malmoe, Sweden

**Correspondence**
Dr. Jalal Taneera
Sharjah Institute for Medical Research
University of Sharjah
27272 Sharjah
United Arab Emirates
jtaneera@sharjah.ac.ae

⊕ **Supplementary Material** for this article is available online at http://www.thieme-connect.de/products.

## ABSTRACT

Silencing of *Chl1* gene expression has been previously reported to reduce insulin secretion. Nevertheless, the mechanism underlying this effect remains unclear. In this study, we performed a serial of studies to investigate how *Chl1* affects insulin secretion in INS-1 cells. RNA-sequencing was used to investigate the expression of *CHL1* in human adipose, liver, muscle, and human islets. Silencing of *Chl1* in INS-1 cells was done to assess its impact on the insulin secretion, content, cell viability, and apoptosis. In addition, gene set enrichment analysis (GSEA) was performed to identify possible molecular signatures that associate with *Chl1* expression silencing. RNA sequencing data revealed a high expression of *CHL1* in pancreatic islets and adipose tissues compared to liver and muscles tissues. Diabetic islets exhibited a lower expression of *CHL1* as compared to non-diabetic islets. *CHL1* expression was found to correlate positively with insulin secretory index, *GLP1R* but inversely with $HbA_{1c}$ and BMI. Silencing of *Chl1* in INS-1 cells markedly reduced insulin content and secretion. The expression of key molecules of β-cell function including *Insulin, Pdx1, Gck, Glut2,* and *Insrβ* was down-regulated in *Chl1*-silenced cells at transcriptional and translational levels. Cell viability, apoptosis, and proliferation rate were not affected. GSEA showed that the insulin-signaling pathway was influenced in *Chl1*-silenced cells. Silencing of *Chl1* impairs β-cell function by disrupting the activity of key signaling pathways of importance for insulin biosynthesis and secretion.

## ABBREVIATION

| | |
|---|---|
| *Chl1* | cell adhesion molecule L1 like |
| T2D | type 2 diabetes |
| siRNA | small interfering RNA |
| $HbA_{1c}$ | hemoglobin A1c |
| GSEA | Gene set enrichment analysis |
| BMI | body mass index. |

## Introduction

The *CHL1* gene encodes a type I transmembrane protein, which belongs to L1 family of cell adhesion molecules (*L1-CAMs*). *CHL1* plays a crucial role in neuronal development [1] where it is highly expressed in various neuronal tissues including neurons, astrocytes, oligodendrocytes, and Schwann cells [2]. *CHL1* has been shown to regulate neurite outgrowth and neuronal migration during brain development [3]. In mature neurons, *CHL1* accumulates in the axonal membrane where it is found to play a vital role in the regula-

tion of synapse function [4]. Moreover, *CHL1* was revealed to be involved in general cognitive activities and neuropathologies including schizophrenia [5–7]. Several reports have suggested that *CHL1* could function as a putative tumor suppressor gene as its expression has been found to be reduced in breast, colon, rectum, thyroid, kidney and small intestine cancers [8]. Additionally, it has been implicated in the regulation and activation of gamma-aminobutyric acid (GABA) as part of the regulation and activation of the MAP/ERK pathway [9].

In a previous study, we reported that silencing of *Chl1* in the clonal rat β-cells INS-1(832/13) reduced glucose-stimulated insulin secretion [10]. However, the mechanism by which *Chl1* gene affects insulin secretion is not well defined. In the current study, the expression of *Chl1* in human pancreatic islets (with/without diabetes), as well as liver, adipose, and muscle, was investigated using RNA-sequencing expression data. More, several functional studies were performed to evaluate the impact of *Chl1* silencing on insulin biosynthesis, insulin secretion, cell viability, apoptosis, and expression of key β-cell function genes. Additionally, microarray gene expression was performed to elucidate the molecular signature associated with *Chl1* silencing in INS-1 cells.

## Materials and Methods

### Isolation of human tissues and pancreatic islets

All examined tissues including islets, liver, adipose (visceral fat, dissected from the pancreas or area close to the pancreas), and muscle tissues were obtained from cadaver donors of European ancestry by the Nordic Islet Transplantation Program. Pancreatic islets were obtained from 172 nondiabetic and 32 type 2 diabetic (T2D) donors and processed as previously described [11, 12]. The characteristics of human islets are shown in ▶ **Table 1**. All procedures in this study were approved by the local ethics committees at Uppsala and Lund universities, Sweden.

### Insulin secretion from isolated islets

Islets were hand-picked under a stereomicroscope at room temperature and pre-incubated for 30 min at 37 °C in Krebs-Ringer bicarbonate (KRB) buffer, pH 7.4, supplemented with 10 mM HEPES, 0.1 % BSA and 1.0 mM glucose. Then, the buffer was changed and the islets were incubated at the indicated glucose concentrations for 60 min at 37 °C. Each incubation sample vial contained 12 islets in 1.0 ml of buffer solution. An aliquot of the medium was removed for insulin release analysis.

### Expression of *Chl1* in human tissue analyzed by RNA-sequencing

Total RNA was isolated from adipose, liver, muscle tissues and pancreatic islets from human cadaveric donors. RNA-sequencing samples were prepared using Illumina's TruSeq RNA Kit. The resulting libraries were checked for quality using the 2200 TapeStation System (Agilent Technologies, USA). Next, every 6 samples were pooled for sequencing on one lane of a Flow cell on a HiSeq 2000 Sequencing System (Illumina, USA). The output reads were aligned to the human reference genome (hg19) with STAR. Raw data were normalized using trimmed mean of M-values and presented as

Fragments Per Kilobase of Exon Per Million Fragments Mapped (FPKM) or transformed into log2 counts per million using the voom-function (edgeR/limma R-packages).

### Cell culture

INS-1 (831/13) cells were maintained in RPMI 1640 culture medium containing 11 mM D-glucose, 10 % fetal bovine serum, 100 units/ml penicillin, 100 µg/ml streptomycin, 10 mM glutamine, 1 mM sodium pyruvate, 10 mM HEPES, and 50 µM β-mercaptoethanol (All from Sigma-Aldrich, Germany) at 37 °C in a humidified atmosphere of 95 % air and 5 % $CO_2$.

### RNA interference and insulin secretion

Clonal β-cells were transfected as previously described [10]. Briefly, 24 h prior to transfection cells were seeded in 24-well plate with a density of 250 000/well in RPMI 1640 medium. The cells were transfected with two different siRNA sequences (s137135 and s137136) (40nM) targeting *Chl1* (ThermoFisher, USA) using lipofectamine RNAiMAX transfection reagent (ThemroFisher). Silencer Negative Control #2 (ThermoFisher) was used. Insulin secretion assay was performed after 48 h of transfection. Briefly, confluent plates were washed twice with 1 mL of pre-warmed Secretion Assay Buffer (SAB), pH 7.2 (114 mM NaCl, 4.7 mM KCl, 1.2 mM $KH_2PO_4$, 1.16 mM $MgSO_4$, 20 mM HEPES, 2.5 mM $CaCl_2$, 25.5 mM $NaHCO_3$ and 0.2 % Bovine Serum Albumin) containing 2.8 mM glucose. Then, cells were incubated for 2 h in fresh 2 mL SAB with 2.8 mM glucose. Later on, separate wells were incubated for 1 h in 1 mL SAB containing either 2.8 mM glucose plus secretagogue; either 16.7 mM glucose, 35 mM KCL or 10 mM α-ketoisocaproic acid (α-KIC). The amount of Na ions was reduced in the SAB buffer to compensate for the addition of 35 mM KCL. The secreted insulin in the supernatant incubation medium was determined using Rat insulin ELISA Kit (Elabscience). Regarding the insulin content assay, total protein was extracted using M-PER Mammalian Protein Extraction Reagent (ThermoFisher Scientific, USA) and quantified by Pierce BCA protein assay kit (ThermoFisher). The total protein was diluted (1:250) and insulin content was determined using rat insulin ELISA kit (Elabscience, China). Finally, insulin content was normalized to total amount of protein.

### RT-qPCR and knockdown efficiency

RNA was extracted using the RNeasy Mini Kit (Qiagen, Germany), after which RNA quality and concentration were assessed using an Agilent 2100 Bioanalyzer (Agilent Biotechnologies, USA) and Nanodrop ND-2000 (ThermoFisher Scientific, USA). cDNA was synthesized using RevertAid H Minus First Strand cDNA synthesis Kit (ThermoFisher Scientific, USA). Gene expression quantification was carried out using TaqMan protocol in Quantstudio3 real-time PCR

▶ **Table 1**   Characteristics of human pancreatic donors.

| | **Non-diabetic donors** | **Type 2 diabetic donors** |
|---|---|---|
| *n* (male/female) | 172 (104/68) | 32 (21/11) |
| Age (years) | 58.8 ± 10 | 61.1 ± 10 |
| BMI (kg/m²) | 26.2 ± 3.8 | 27.9 ± 4.5 |
| HbA1c | 5.8 ± 0.6 | 6.8 ± 0.8 |

machine (Applied Biosystems, USA) using gene-specific primer probes for *Chl1* (Rn01420997_m1), *Ins1* (Rn01774648_g1), *Ins2* (Rn02121433_g1), *Mafa* (Rn00845206_g1), *Pdx1* (Rn00755591_m1), *Insr* (Rn00690703_m1) and *Gck* (Rn00561265_m1) (All from Applied Biosystems, USA). Rat Hprt (Applied Biosystems, USA) was used to normalize gene expression by the ΔCt method and the final normalized quantity was expressed as $2^{-\Delta\Delta Ct}$.

## Cell viability and cell counting assays

The colorimetric assays MTT (3-(4,5-dimethylthiazol-2-yl)-2,5-diphenyltetrazolium bromide) (Sigma-Aldrich, Germany) and XTT (sodium 3´-[1-(phenylaminocarbonyl)- 3,4-tetrazolium]-bis (4-methoxy6-nitro) benzene sulfonic acid hydrate) (Roche Diagnostics) ) were used as to assess cell viability and metabolism. For cell counting, INS-1 cells were seeded in 96-well plates at a density of 20 000 cells/well in 0.2 mL of RPMI complete medium and incubated overnight. The cells were transfected with siRNAs against *Chl1* or negative control. The transfected cells were harvested by trypsinization and the number of viable cells was counted using a hemacytometer after staining cells with trypan blue dye. The MTT and XTT assays were performed at 48 h post-transfection. Briefly, 20 μl MTT solution (5 mg/mL stock) was added to each well and incubated for 4 h at 37 °C. The medium was removed and the formed formazan crystals were dissolved in 150 μL of dimethyl sulfoxide (DMSO). The absorbance was recorded using a microplate reader (Biotek, VT, USA) at a wavelength of 570 nm. For XTT assay, 50 μL of the XTT labeling mixture (Roche Diagnostics) was added to each well and incubated for 4 h at 37 °C and absorbance was recorded at 450 nm. The percentage of cell viability was calculated from the average absorbance value (nm) using the formula: % cell viability = (OD absorbance (nm) of *Chl1* silenced cells / OD absorbance (nm) of siRNA negative control) × 100.

## Apoptosis and proliferation analysis

Apoptosis analysis was performed 48 h post-transfection. Cells were harvested and re-suspended in 500 μl of Annexin-V (1X) binding buffer (BD Biosciences, USA) containing a 5 μl of Annexin V-FITC and 5 μl Propidium Iodide. Samples were incubated at room temperature for 10 min and then analyzed by flow cytometry (FACSAria III, BD Biosciences, USA). Cell proliferation was measured using the (5(6)-Carboxyfluorescein N-hydroxysuccinimidyl ester (CFSE) labeling. Briefly, cells were incubated with 1 μM CFSE dye (ThermoFisher Scientific, USA) for 10 min and then subjected to siRNA transfection as explained above. The analysis was done on flow cytometry (FACSAria III, BD Biosciences, USA) after 0, 24 or 48 h.

## Western blot analysis

Total protein was extracted from transfected cells using M-PER™ Mammalian protein extraction reagent (ThermoFisher Scientific, USA) containing protease inhibitor cocktail (ThermoFisher Scientific, USA). A 50 μg of protein lysate was separated on 10 % sodium dodecyl sulfate-polyacrylamide gel electrophoresis (SDS-PAGE) and transferred onto a nitrocellulose membrane (Bio-Rad, USA). The membranes were blocked with 5 % skimmed milk prepared in Tris-buffered saline with 0.1 % of Tween 20 (TBST) for 1 h at room temperature. The blot was probed with antibodies against *Chl1*

(Anti-rabbit; 1:1000; #C411215, Lifespan Biosciences, USA), Insulin (Anti-mouse; 1:1000; #8138s, Cell signaling Technology, USA), INSRα (Anti-rabbit; 1:1000; #ab5500, Abcam, UK), INSRβ (Anti-mouse; 1:1000; #ab69508, Abcam, UK), PDX1 (Anti-rabbit; 1:3000, #ab47267, Abcam, UK), GLUT2 (Anti-rabbit; 1:1000, #ab54460, Abcam, UK), GCK (Anti-rabbit; 1:500; #ab37796, Abcam, UK) or β-actin (1:5000; #A5441, Sigma-Aldrich, Germany) for overnight at 4 °C. The secondary antibodies (anti-mouse #7076S and anti-rabbit #7074S, Cell signaling Technology, USA) were then reacted with the membrane at 1:1000 dilutions for 1 h at room temperature. Chemiluminescence was detected using the ECL substrate kit (Bio-Rad, USA). Protein bands were detected using the Bio-Rad Image Lab software (ChemiDoc Touch Gel Western Blot Imaging System; Bio-Rad, USA) and bands were quantified using Image J software. β-actin was used as endogenous control.

## Microarray gene expression in INS-1 cells

The microarrays were performed using the Affymetrix standard protocol. Briefly, 100–200 ng of total RNA were processed according to instructions of the GeneChip® Expression 3'-Amplification Reagents One-cycle cDNA synthesis kit (Affymetrix, ThermoFisher Scientific, USA) to produce double-stranded cDNA. This was used as a template to generate biotin-targeted cRNA following manufacturer's specifications. 15 μg of biotin-labeled cRNA was fragmented to strands between 35 and 200 bases in length, after which 10 μg were hybridized onto the GeneChip® Rat Gene 2.0 ST whole transcript based assay overnight in the GeneChip® Hybridization oven 6400 using standard procedures. Arrays were washed and stained in a GeneChip® Fluidics Station 450. Scanning was carried out with the GeneChip® Scanner 3000 and image analysis was performed using GeneChip® Operating Software. Array data were summarized and normalized with Robust Multi-Array Analysis (RMA) method.

## Absolute Gene Set Enrichment Analysis (absGSEA)

Microarray data underwent pre-processing and normalization through affy-package RMA Bioconductor, R statistical software version 3.0.2. A mathematical model was used to identify the genes that are differentially expressed between *Chl1*-silenced cells and controls. absGSEA method was applied on the normalized data to identify a novel subset of genes and pathways that are enriched significantly as previously described in around 10,000 cellular pathways using the Kolmogorov-Smirnoff test [13, 14]. The Benjamini–Hochberg method was used for error correction (q-value calculation).

## Statistical analysis

We used edge-R to calculate differential gene expression (adjusted for age, sex, and BMI) in human islets. For the potential correlation between genes and association between gene expression and phenotypes, the data were calculated by Spearman's correlation. P-values illustrating the significance were calculated using the eBayes function in limma [15]. For insulin secretion and qRT-PCR analysis, we used a parametric unpaired two-tailed Student's t-test. Data are presented as mean ± SEM unless otherwise stated. Statistical significance was indicated by asterisks ($*p < 0.05$, $**p < 0.01$, $***p < 0.001$).

Taneera J et al. Reduced Expression of CHL1 … Exp Clin Endocrinol Diabetes 2019; 127: 1–9

3

# Results

## RNA expression analysis of *Chl1* in human pancreatic islets and metabolic tissues

Analysis of *CHL1* expression in metabolic tissues obtained from cadaveric human organ donors showed a higher expression level of *CHL1* in adipose tissues and lower expression level in muscle tissues as compared with pancreatic islets (▶ **Fig.1a**). Further analysis of *CHL1* expression using RNA sequencing data from a large number of human islets (n = 172) showed relatively lower expression levels (top 21st percentile of genes expressed) (▶ **Fig. 1b**) when compared to the ion channel gene KCNJ11; a high expression functional marker in human islets [16]. Previously, we have shown that *CHL1* is reduced in diabetic islets as compared to non-diabetic using Affymetrix microarray expression obtained from 63 donors [10]. In the present study, we replicated the finding using different technology (RNA-sequencing) on large number of donors (n = 181). RNA-sequencing median expression of *CHL1* showed significant lower expression (p = 0.00006; adjusted for age, sex and BMI) in donors with type 2 diabetes (T2D; HbA1c ≥ 6.5 %) compared to non-diabetic (HbA1c < 6 %) or IGT (impaired glucose tolerant donors; 6 % ≤ HbA1c < 6.5) (▶ **Fig. 1c**). Moreover, expression of *CHL1* correlated negatively with $HbA_{1c}$ and BMI (▶ **Fig. 1d, f**) but correlated positively with insulin secretion and *GLP1R* (▶ **Fig. 1e, g**). Additionally, *Chl1* expression was investigated using previously published RNA-sequencing expression data from sorted human pancreatic endocrine cells [17]. There was a 2.5-fold increase in the *CHL1* expression in pancreatic β-cells compared to α-cells as well as a 4-fold increase when compared to exocrine cells (data not shown).

## *Chl1* reduces insulin secretion and content in INS-1 cells

In previous work, we have reported that silencing of *Chl1* in INS-1 cells reduced insulin secretion [10]. However, the impact of *Chl1* silencing on the exocytosis machinery or mitochondrial metabolism is not known. To this end, we silenced the expression of *Chl1* in clonal INS-1 cells using a pool of tow siRNA sequences. Silencing efficiency of *Chl1* expression was assessed 48 hr post-transfection by qRT-PCR, where it was almost 50 % relative to the negative control (p < 0.01) (▶ **Fig. 2a**). This was further confirmed by western blotting (▶ **Fig. 2d**). In support of previous results, glucose-stimulation of insulin secretion (GSIS) with 2.8 or 16.7 mM glucose in *Chl1*-silenced cells was markedly reduced as compared with siRNA negative control (~45 %; p < 0.01) (▶ **Fig. 2b**). Stimulation of *Chl1*-silenced cells with 2.8 mM glucose in the presence of 10 mM α-KIC, a secretagogue that directly stimulates mitochondrial metabolism, or 35 mM KCL (a membrane-depolarizing agent), showed no effect as compared with negative controls (▶ **Fig. 2b**). Additionally, we observed a significant reduction of insulin content in *Chl1*-silenced cells (~25 %; p < 0.05) (**not shown**).
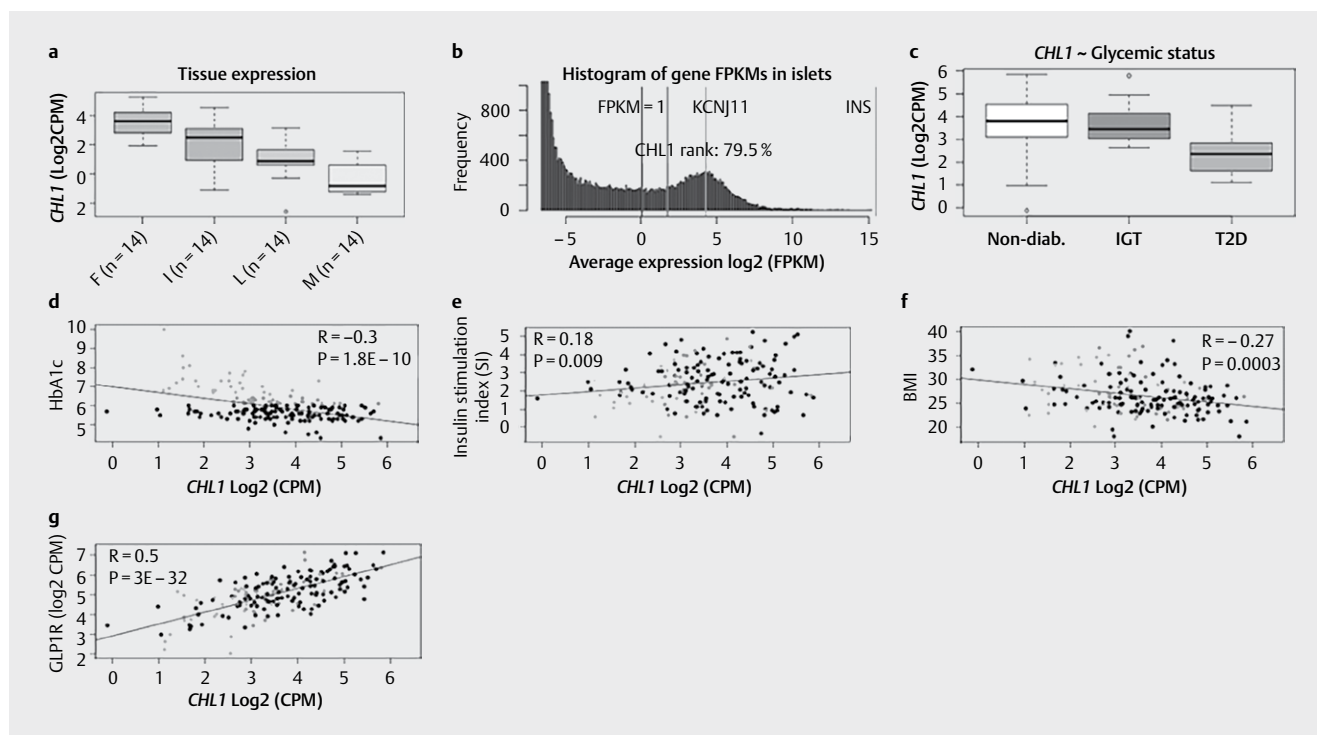


▶ **Fig. 1** RNA-sequencing expression of *Chl1* in human pancreatic islets and metabolic tissues. **a** Expression of *Chl1* transcripts in human adipose/fat tissue (F) (n = 14), pancreatic islets (I) (n = 14), liver (L) (n = 14) and skeletal muscle tissues (M) (n = 14) as revealed by RNA-seq. **b** RNA-seq expression data from non-diabetic human islets (n = 172) showing a histogram of *Chl1* expression frequency (FPKMs) as compared to *KCNJ11* and *Insulin* genes as an expression marker. **c** Comparison of RNA-sequencing normalized median expression of *Chl1* in pancreatic islets of non-diabetic (n = 146), IGT (n = 19), and T2D corresponds with diabetic donors (n = 16). (D-G) Spearman's correlation of *Chl1* with $HbA_{1c}$ (n = 181) **d**, insulin stimulation index (n = 196) **e**, BMI (n = 202) (F) and *GLP1R* (n = 202) **g** performed on human islets RNA-sequencing data. Black points represent non-diabetic donors, blue points represent IGT donors and grey points represent donors with T2D. The data were analyzed with linear regression; p values are indicated in the respective graphs (n = 192). Bars represent mean ± SEM.
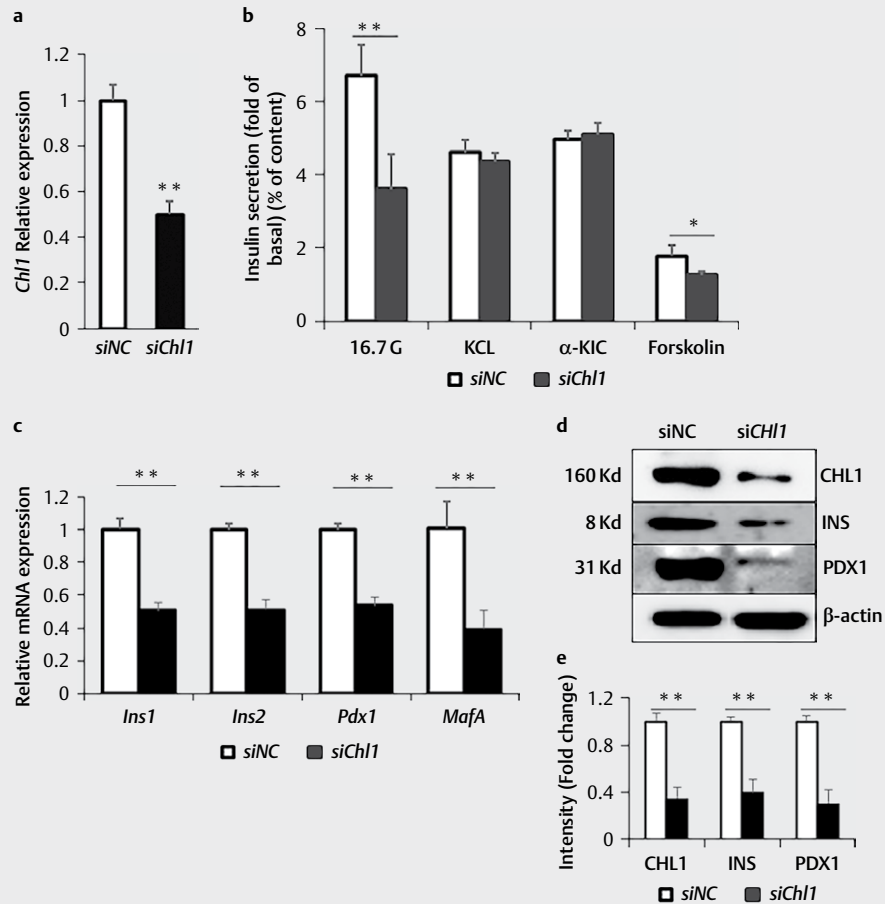
▶ **Fig. 2**  Impact of *Chl1* silencing in INS-1 (832/13) cells on insulin secretion and genes involved in β-cell function. **a** Silencing efficiency of siRNA of *Chl1* in INS-1 cells (832/31). **b** Normalized insulin secretion in response to 2.8 and 16.7 mM glucose and 10 mM a-KIC (+2.8 mM glucose), 35 mM potassium chloride (KCL) (+2.8 mM glucose) or 10μM forskolin (+2.8 mM glucose). Secretion was expressed as a fold increase (insulin secreted at 16.7 mM glucose/insulin secreted at 2.8 mM glucose). **c** RT-qPCR expression analysis of *Ins1*, *Ins2*, *Pdx1*, and *Mafa* in *Chl1*-silenced cells relative to control. **d** Western blot analysis of *Chl1*, Insulin, and PDX1 in comparison to the endogenous control β-actin from *Chl1*-silenced cells and negative siRNA control. **e** Fold change differences in intensity of western blot bands of *Chl1*, Insulin and PDX1 protein expression relative to β-actin. All shown data were from 3–5 independent experiments in triplicate. Bars represent mean ± SD.

In view of the positive correlation of *GLP1R* with *Chl1* (▶ **Fig. 1g**), we tested whether silencing of *Chl1* impaired insulin secretion via cAMP production. As shown ▶ **Fig 2b**, insulin secretion in response to 2.8 mM glucose + forskolin (activator of adenylyl cyclase that increases the intracellular cAMP levels) was reduced (p > 0.05) as compared to the negative control.

## Silencing of *Chl1* affects the expression of genes involved in β-cell function, but not cell viability in INS-1 cells

A significant reduction in mRNA expression of the proinsulin genes *Ins1* and *Ins2* (p < 0.01) in *Chl1*-silenced cells was observed as compared to the negative control (▶ **Fig. 2c**). Moreover, the mRNA expression of the insulin-regulator transcription factors, *Pdx1* and *Mafa*, was significantly down-regulated (p < 0.001) in *Chl1*-silenced cells (▶ **Fig 2c**). Western blot analysis showed almost 60 % reduction of Insulin expression and 75 % reduction of PDX1 expression (p < 0.01) (▶ **Fig. 2d-e**).

To clarify whether *Chl1*-silencing affects apoptosis or cell viability, the *Chl1*-silenced cells were evaluated by MTT, XTT and cell counting. As illustrated in ▶ **Fig. 3a** and b, no significant differences were observed by MTT and XTT assays. Cell counting showed a slight reduction (p = 0.09) between *Chl1*-silenced cells and negative control cells (▶ **Fig. 3c**). Annexin-V/PI staining was performed to discriminate necrotic/dead cells from apoptotic cells. As shown in ▶ **Fig. 3d**, a minor level of apoptosis (not significant) was observed in *Chl1*-silenced INS-1 cells as compared with negative control cells. Furthermore, there was no difference in the proliferative response between *Chl1*-silenced cells as compared with siRNA negative controls at 24 or 48 hr post-transfection as assessed with CFSE (▶ **Fig. 3e**).

## Enrichment for insulin signaling pathway in *Chl1*-silenced INS-1 cells

Microarray expression analysis showed that 100 genes were differentially expressed (p < 0.005) in *Chl1*-silenced INS-1 cells, out of

Taneera J et al. Reduced Expression of CHL1 ...  Exp Clin Endocrinol Diabetes 2019; 127: 1–9

5
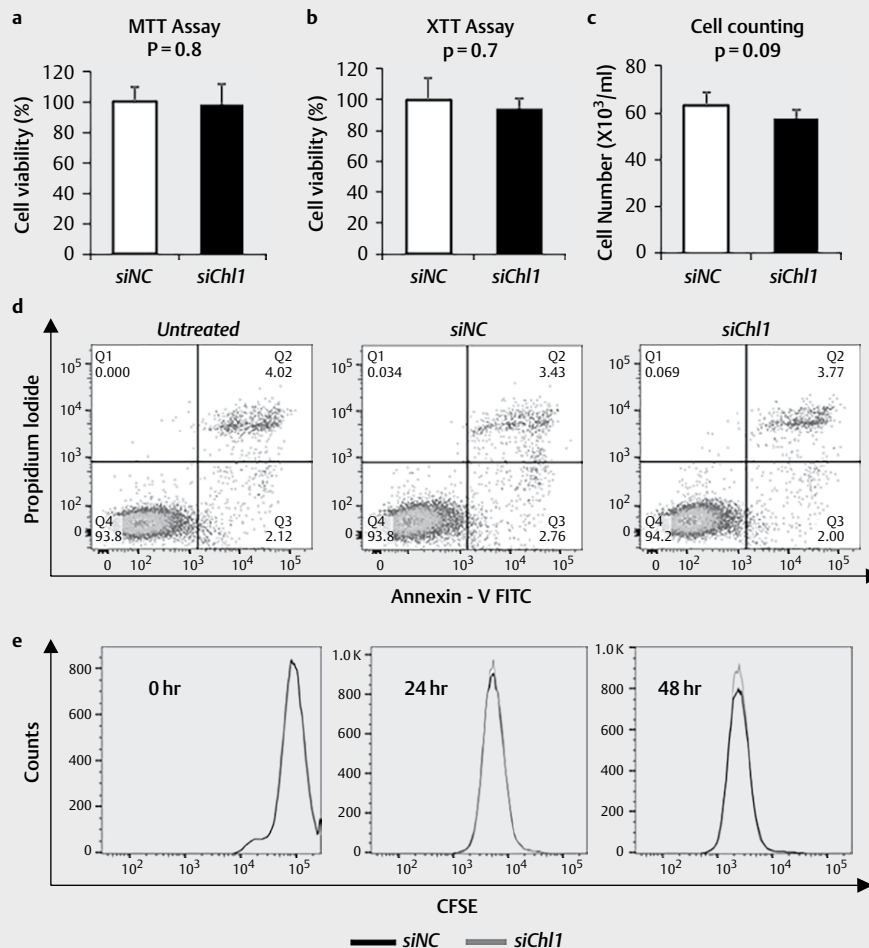
▶ **Fig. 3** Effect of *Chl1* silencing on cell viability and apoptosis. **a** Percentage of cell viability was determined using the MTT assay, from three independent experiments in triplicate. **b** Percentage of cell viability was determined using the XTT assay, with n = 8 in each group. **c** Cell counting in *Chl1*-silenced INS-1 cell compared to the negative control, with n = 8 in each group. **d** Assessment of apoptosis in *Chl1*-silenced cells, siRNA negative control or untreated cells as analyzed by flow cytometry. Data are representative of 3 independent experiments. **e** Assessment of cell proliferation using CFSE staining in *Chl1*-silenced INS-1 cells as determined compared to siRNA negative control. Data were obtained from a pool of 3 independent experiments. Bars represent mean ± SD

which 57 were up-regulated and 43 were down-regulated. *Srp14, Ptbp2, Gria2, Kcnd2,* and *Vps26a* were the top up-regulated genes while *Serpina6, Emp1, Klk1, Rnf186,* and *Aqp5* were the top 5 down-regulated genes (▶ **Table 1S, 2S**). As none of these genes has been previously implicated in insulin secretion, we performed Absolute GSEA to gain insight into the potential enriched cellular pathways in *Chl1*-silenced cells. Absolute GSEA (absGSEA) approach was utilized as it has the potential to identify up-regulated and down-regulated genes within a given enriched pathway [18]. We explored 1318 differentially expressed genes where the cut-off was p < 0.05. Then, pathways that passed the AbsGSEA filtration were explored using GSEA. Hence, out of the 6000 cellular pathways that passed the AbsGSEA, 174 were enriched between *Chl1*-silenced cells and negative control cells (▶ **Table 3S**). RAS and ERK signaling pathways were among the top enriched pathways (▶ **Tables 3S**), where both pathways were reported to regulate neuronal migration involving cell adhesion molecules [19]. Interestingly, KEGG insulin signaling

pathway was over-re-presented in the *Chl1*-silenced cells. A heat-map illustration of the KEGG insulin signalling pathways displayed 6 genes to have an enhanced enrichment (*Ppargc1a, Prkx, Prkaa2, Ptpn1, Pik3ca,* and *Phkg1*) whereas 12 genes were down-regulated (*Pik3r5, Foxo1, Ikbkb, Ppp1r3b, Ppp1r2a, Gck, Shc1, Flot2, Insr, Srebf1, Nras,* and *Kras*) (▶ **Fig. 4a** and ▶ **Table 2**).

To validate the microarray data, we performed RT-qPCR and western blot expression analysis for *Gck* and *Insr*. As shown in ▶ **Fig. 4b** and **c**, a significant reduction in the mRNA expression of *Gck* (36 %) and Insr (22 %) was evident (p < 0.05). Likewise, western blotting data showed a 60 % reduction of GCK and INSRβ expression of GCK (▶ **Fig 4e, f** and **h**). No change was observed on INSRα protein expression (▶ **Fig 4f** and **h**). Moreover, the mRNA expression of the glucose transporter 2 (*Glut2*) showed a significant down-regulation in *Chl1*-silenced cells (▶ **Fig 4d**), which was further confirmed by protein studies (▶ **Fig 4g-h**).
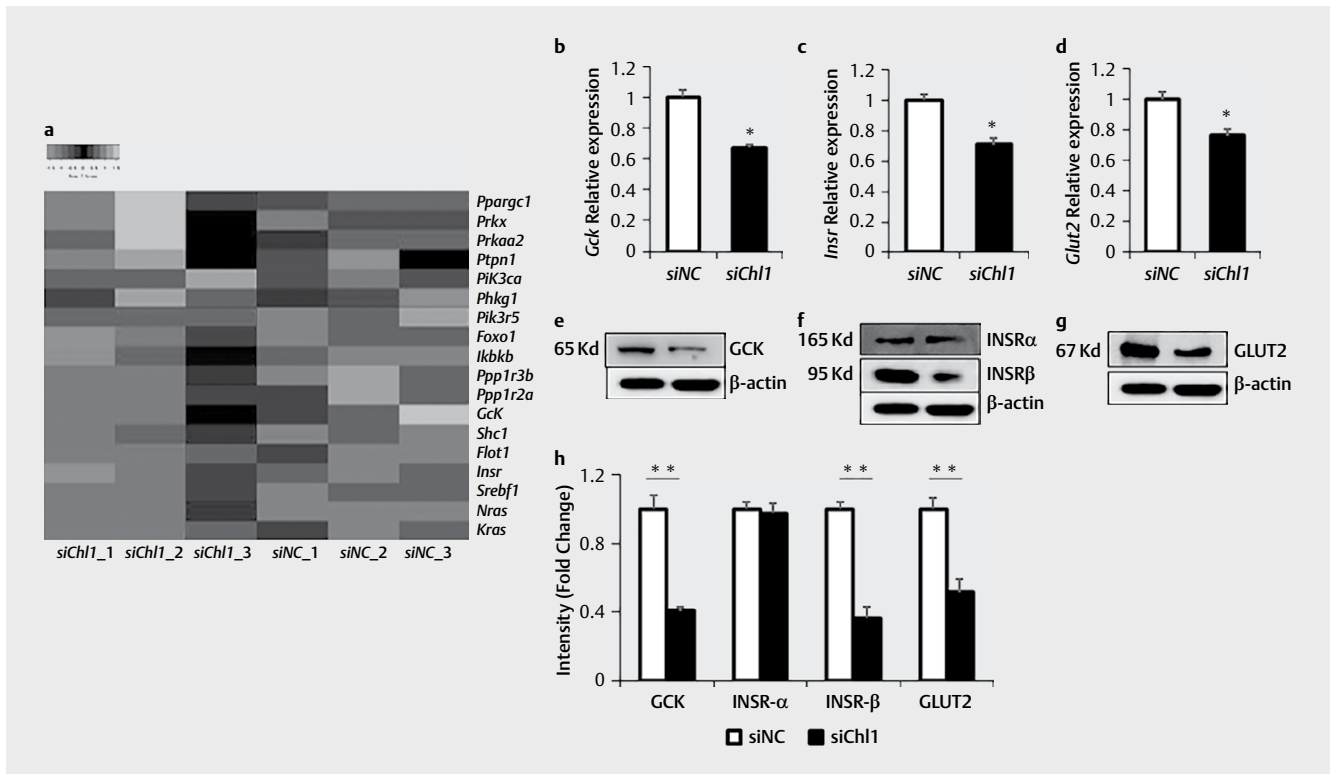
► **Fig. 4** GSEA and expression of differentially expressed genes. **a** Heatmap for the differentially expressed members of KEGG insulin signaling pathway between *Chl1* silenced cells (*n* = 3) and scrambled negative control (*n* = 3). Red color indicates the upregulated genes and green color downregulated genes. **b-d**) RT-qPCR expression of *Gck* **b**, *Insr* **c** and *Glut2* **d** in *Chl1* silenced cells relative to a negative control. RT-qPCR data were obtained from three independent experiments in triplicate **e-g** Western blot expression of GCK **e**, INSRα/ INSRβ **f**, and GLUT2 **g**) in *Chl1* silenced cells relative to the negative control. **h** Fold change differences in intensity of western blot bands in GCK, INSRα, INSRβ, GLUT2 protein expression (► **Figs. 4e, f** and g) relative to β-actin. Bars represent mean ± SD.

## Discussion

In the current study, our findings shed more light on the potential role of *CHL1* in pancreatic β-cell function. The *CHL1* gene is highly expressed in islets where its expression was found to correlate positively with insulin secretion and negatively with $HbA_{1c}$ and BMI. The observed differential expression pattern of *CHL1* in diabetic and non-diabetic human islets is consistent with previously published data [10]. Given that elevated $HbA_{1c}$ is a marker of poorly regulated blood sugar levels and impaired β-cell function [20], its negative correlation with *CHL1* is additional evidence of the positive role of *CHL1* in glucose metabolism. On the other hand, increased BMI is a marker of impaired glucose metabolism [21], and thus the negative correlation between *CHL1* and BMI suggests a positive role of *CHL1* in β cell function in man. As illustrated in ► **Fig. 1**, *CHL1* was highly expressed in the adipose tissue. This was interesting as adipose tissue is one of the vital metabolic organs where the secreted insulin exerts its effect by accelerating glucose uptake to maintain blood sugar within the physiological range.

The positive impact of *CHL1* expression on β-cell function is consistent with previous studies that have reported cell adhesion molecules and receptors to be essential for islet function [22, 23]. For example, the neural cell adhesion molecule (*Ncam*) was shown to play a key role in islet cell type segregation via affecting the distribution of F-actin and cadherins [22, 24]. It is worth noting that *Chl1*

and *Ncam* are members of the transmembrane immunoglobulin (Ig) superfamily, where *Chl1* activates the ERK pathway through *Src*. *Ncam* stimulates the recruitment of tyrosine kinase *Fyn* to activate Fak, ERK and the transcription factor cAMP response element-binding protein (CREB) [19]. Hence, this might explain the reported microarray finding that reduced *Chl1* expression is associated with ERK pathway enrichment. Despite the fact that *Chl1* was reported to act as a neuronal survival factor in cerebellar and hippocampal neurons [25], our data showed that *Chl1* silencing in INS-1 cells was not associated with altered survival or apoptosis. Although the expression of *CHL1* is frequently increased in some (lung, ovary, uterus, liver, and trachea) cancers, it is frequently reduced in many other cancers (breast, kidney, rectum, colon, thyroid, stomach, skin, small intestine, bladder, vulva and pancreatic cancer) [8]. This suggests that the role of *Chl1* in cell survival is perhaps cell/ microenvironment dependent.

In this study, we aimed to investigate the collective impact of *Chl1*-silencing on the insulin secretory machinery. Our data suggest that GSIS and insulin are reduced. This was accompanied by a reduction of the expression of *Ins1, Ins2, Pdx1,* and *Mafa*, which further supported that *CHL1* is an important player in insulin secretion. The upstream pathway analysis suggests that the *Chl1* silencing affect insulin receptor signaling pathways. This was in line with previous reported data where silencing of *Ncam* was found to re-

Taneera J et al. Reduced Expression of CHL1 … Exp Clin Endocrinol Diabetes 2019; 127: 1–9

7

▶ **Table 2** List of the differential expressed genes in insulin signaling pathway.

| ID | Chl1 Avg (log2) | CTRL Avg (log2) | Fold Change | P-val | q-val | Gene Symbol | Description |
|---|---|---|---|---|---|---|---|
| 17690210 | 9.07 | 8.53 | 1.45 | 0.0023 | 0.3364 | Ppargc1a | peroxisome proliferator-activated receptor gamma, coactivator 1 alpha |
| 17877458 | 9.39 | 8.94 | 1.37 | 0.0076 | 0.3872 | Prkx | protein kinase, X-linked |
| 17808996 | 8.42 | 8.04 | 1.3 | 0.0156 | 0.4294 | Prkaa2 | protein kinase, AMP-activated, alpha 2 catalytic subunit |
| 17769213 | 10.45 | 10.17 | 1.22 | 0.0408 | 0.5147 | Ptpn1 | protein tyrosine phosphatase, non-receptor type 1 |
| 17737691 | 9.87 | 9.7 | 1.13 | 0.0353 | 0.4996 | Pik3ca | phosphatidylinositol-4,5-bisphosphate 3-kinase, catalytic subunit alpha |
| 17677250 | 8.48 | 8.33 | 1.12 | 0.033 | 0.4967 | Phkg1 | phosphorylase kinase, gamma 1 |
| 17647186 | 6.09 | 6.34 | −1.19 | 0.012 | 0.4009 | Pik3r5 | phosphoinositide-3-kinase, regulatory subunit 5 |
| 17738449 | 10.49 | 10.79 | −1.23 | 0.0419 | 0.5173 | Foxo1 | forkhead box O1 |
| 17708867 | 8.99 | 9.29 | −1.23 | 0.0176 | 0.4381 | Ikbkb | inhibitor of kappa light polypeptide gene enhancer in B-cells, kinase beta |
| 17712099 | 9.08 | 9.42 | −1.26 | 0.0084 | 0.3872 | Ppp1r3b | protein phosphatase 1, regulatory subunit 3B |
| 17847758 | 9.76 | 10.1 | −1.27 | 0.0241 | 0.4668 | Pppar2a | protein kinase, cAMP dependent regulatory, type II alpha |
| 17696054 | 8.26 | 8.62 | −1.28 | 0.0161 | 0.431 | Gck | glucokinase |
| 17740110 | 9.8 | 10.17 | −1.29 | 0.0054 | 0.3739 | Shc1 | SHC (Src homology 2 domain containing) transforming protein 1 |
| 17648819 | 9.17 | 9.73 | −1.47 | 0.0289 | 0.4856 | Flot2 | flotillin 2 |
| 17671354 | 8.98 | 9.55 | −1.48 | 0.0152 | 0.4271 | Insr | insulin receptor |
| 17656772 | 9.1 | 9.72 | −1.53 | 0.0181 | 0.44 | Srebf1 | sterol regulatory element binding transcription factor 1 |
| 17741458 | 10.49 | 11.18 | −1.61 | 0.0007 | 0.2877 | Nras | neuroblastoma ras oncogene |
| 17796369 | 8.33 | 9.56 | −2.34 | 0.0216 | 0.4545 | Kras | Kirsten rat sarcoma viral oncogene |

duce insulin signaling in pre-adipocyte cells [26]. Among the differential expressed genes in the insulin-signaling pathway in Chl1-silenced cells, is Gck (Glucokinase), which has a high Km for glucose and is associated with maturity-onset diabetes of the young (MODY) and T2D [27, 28]. In the present investigation, both microarray and RT-qPCR expression analysis showed reduced mRNA expression of Gck. Another notable finding was the reduced expression of insulin receptor Insr, and Glut2 at both mRNA and protein levels in Chl1-silenced cells. A recent study has reported that the Insr knockdown phenotype in pancreatic β-cells was associated with reduced expression of Glut2 and Pdx1 genes and hence decreased insulin secretion [29]. Thus, the down-regulation of Insr in Chl1-silenced cells might lessen the translocation of glucose transporter Glut2 and subsequently lower insulin secretion. It is worth mentioning that the main limitations of this study are the efficiency of silencing (~60%) of the Chl1 gene. In addition, RNA-sequencing data address the expression of Chl1 in intact islets rather than sorted pancreatic β and α cells. Lastly, we are not able to perform western blot analysis of CHL1 expression in human islets from both non-diabetic donors and T2D donors due to inaccessibility of diabetic donors.

In conclusion, this study demonstrates that the expression of Chl1 in non-neuronal tissues is important for regulation of whole-body metabolism. Silencing of Chl1 impairs insulin secretion by disrupting the expression of multiple genes involved in insulin biosynthesis/secretion which might also affect its pulsatility pattern [30] where key insulin signaling pathways could be modulated.

## Author Contributions

JT; conceived and designed the experiments. JT, SD, AM, and DM performed all experimental work. JT, RH, and MH analyzed the data; JT, MH and AS wrote and edited the manuscript.

**One Sentence Summary**: CHL1 gene plays an important role in insulin secretion

# Acknowledgments

## Conflicts of Interest

All authors declare that they have no conflict of interest to disclose.

## References

[1] Demyanenko GP, Halberstadt AI, Rao RS et al. CHL1 cooperates with PAK1–3 to regulate morphological differentiation of embryonic cortical neurons. Neurosci 2010; 165: 107–115

[2] Hillenbrand R, Molthagen M, Montag D et al. The close homologue of the neural adhesion molecule L1 (CHL1): Patterns of expression and promotion of neurite outgrowth by heterophilic interactions. Eur J Neurosci 1999; 11: 813–826

[3] Buhusi M, Midkiff BR, Gates AM et al. Close homolog of L1 is an enhancer of integrin-mediated cell migration. J Biol Chem 2003; 278: 25024–25031

[4] Leshchyns' ka I, Sytnyk V. Reciprocal interactions between cell adhesion molecules of the immunoglobulin superfamily and the cytoskeleton in neurons. Front Cell Dev Biol 2016; 4: 9

[5] Shoukier M, Fuchs S, Schwaibold E et al. Microduplication of 3p26. 3 in nonsyndromic intellectual disability indicates an important role of CHL1 for normal cognitive function. Neuropediatrics 2013; 44: 268–271

[6] Montag-Sallaz M, Baarke A, Montag D. Aberrant neuronal connectivity in CHL1-deficient mice is associated with altered information processing-related immediate early gene expression. J Neurobiol 2003; 57: 67–80

[7] Irintchev A, Koch M, Needham LK et al. Impairment of sensorimotor gating in mice deficient in the cell adhesion molecule L1 or its close homologue, CHL1. Brain research 2004; 1029: 131–134

[8] Senchenko VN, Krasnov GS, Dmitriev AA et al. Differential expression of CHL1 gene during development of major human cancers. PloS one 2011; 6: e15612

[9] Huang X, Zhu L-l, Zhao T et al. CHL1 negatively regulates the proliferation and neuronal differentiation of neural progenitor cells through activation of the ERK1/2 MAPK pathway. Mol Cell Neurosci 2011; 46: 296–307

[10] Taneera J, Lang S, Sharma A et al. A systems genetics approach identifies genes and pathways for type 2 diabetes in human islets. Cell Metab 2012; 16: 122–134

[11] Fadista J, Vikman P, Laakso EO et al. Global genomic and transcriptomic analysis of human pancreatic islets reveals novel genes influencing glucose metabolism. Proc Natl Acad Sci USA 2014; 111: 13924–13929

[12] Taneera J, Fadista J, Ahlqvist E et al. Identification of novel genes for glucose metabolism based upon expression pattern in human islets and effect on insulin secretion and glycemia. Hum Mol Genet 2014; 24: 1945–1955

[13] Hamoudi RA, Appert A, Ye H et al. Differential expression of NF-κB target genes in MALT lymphoma with and without chromosome translocation: Insights into molecular mechanism. Leukemia 2010; 24: 1487

[14] Butt MA, Pye H, Haidry RJ et al. Upregulation of mucin glycoprotein MUC1 in the progression to esophageal adenocarcinoma and therapeutic potential with a targeted photoactive antibody-drug conjugate. Oncotarget 2017; 8: 25080

[15] Ritchie ME, Phipson B, Wu D et al. limma powers differential expression analyses for RNA-sequencing and microarray studies. Nucleic acids Res 2015; 43: e47–e47

[16] Jonsson A, Isomaa B, Tuomi T et al. A variant in the KCNQ1 gene predicts future type 2 diabetes and mediates impaired insulin secretion. Diabetes 2009■■

[17] Bramswig NC, Everett LJ, Schug J et al. Epigenomic plasticity enables human pancreatic α to β cell reprogramming. J Clin Invest 2013; 123: 1275–1284

[18] Saxena V, Orgill D, Kohane I. Absolute enrichment: gene set enrichment analysis for homeostatic systems. Nucleic acids Res 2006; 34: e151–e151

[19] Schmid RS, Maness PF. L1 and NCAM adhesion molecules as signaling coreceptors in neuronal migration and process outgrowth. Cur Opi Neurobiol 2008; 18: 245–250

[20] Ligthart S, van Herpt TT, Leening MJ et al. Lifetime risk of developing impaired glucose metabolism and eventual progression from prediabetes to type 2 diabetes: a prospective cohort study. Lancet Diabetes Endocrinol 2016; 4: 44–51

[21] Oh JY, Sung YA, Lee H. The lipid accumulation product as a useful index for identifying abnormal glucose regulation in young Korean women. Diabetic Med 2013; 30: 436–442

[22] Olofsson CS, Håkansson J, Salehi A et al. Impaired insulin exocytosis in neural cell adhesion molecule −/− mice due to defective reorganization of the submembrane F-actin network. Endocrinology 2009; 150: 3067–3075

[23] Dunér P, Al-Amily IM, Soni A et al. Adhesion G protein-coupled receptor G1 (ADGRG1/GPR56) and pancreatic β-cell function. J Clin Endocrinol Metab 2016; 101: 4637–4645

[24] Esni F, Täljedal I-B, Perl A-K et al. Neural cell adhesion molecule (N-CAM) is required for cell type segregation and normal ultrastructure in pancreatic islets. J Cell Biol 1999; 144: 325–337

[25] Chen S, Mantei N, Dong L et al. Prevention of neuronal cell death by neural adhesion molecules L1 and CHL1. J Neurobiol 1999; 38: 428–439

[26] Yang HJ, Xia YY, Wang L et al. A novel role for neural cell adhesion molecule in modulating insulin signaling and adipocyte differentiation of mouse mesenchymal stem cells. J Cell Sci 2011; jcs. 085340

[27] Voight BF, Scott LJ, Steinthorsdottir V et al. Twelve type 2 diabetes susceptibility loci identified through large-scale association analysis. Nature Genet 2010; 42: 579

[28] Vionnet N, Stoffel M, Takeda J et al. Nonsense mutation in the glucokinase gene causes early-onset non-insulin-dependent diabetes mellitus. Nature 1992; 356: 721

[29] Wang J, Gu W, Chen C. Knocking down insulin receptor in pancreatic beta cell lines with lentiviral-small hairpin RNA reduces glucose-stimulated insulin secretion via decreasing the gene expression of insulin, GLUT2 and Pdx1. Int J Mol Sci 2018; 19: 985

[30] Salehi A, Qader SS, Grapengiesser E et al. Inhibition of purinoceptors amplifies glucose-stimulated insulin release with removal of its pulsatility. Diabetes 2005; 54: 2126–2131

Taneera J et al. Reduced Expression of CHL1 ... Exp Clin Endocrinol Diabetes 2019; 127: 1–9

9

# Supplementary Material

▶ **Table 1S** Top up-regulated genes in *Chl1*-silenced cells vs. control.

| Gene symbol | p-value | q-value | FC | Gene Name |
|---|---|---|---|---|
| Srp14 | 0.004 | 0.039 | 2.50 | signal recognition particle 14 |
| Ptbp2 | 0.000 | 0.006 | 1.80 | polypyrimidine tract binding protein 2 |
| Gria2 | 0.002 | 0.014 | 1.72 | glutamate receptor, ionotropic, AMPA 2 |
| Kcnd2 | 0.004 | 0.032 | 1.68 | potassium voltage-gated channel, Shal-related subfamily, member 2 |
| Vps26a | 0.000 | 0.002 | 1.38 | vacuolar protein sorting 26 homolog A (S. pombe) |
| Setd7 | 0.000 | 0.001 | 1.35 | SET domain containing (lysine methyltransferase) 7 |
| Suv420h1 | 0.002 | 0.019 | 1.34 | suppressor of variegation 4–20 homolog 1 (Drosophila) |
| Samd7 | 0.003 | 0.022 | 1.31 | sterile alpha motif domain containing 7 |
| Fam171b | 0.004 | 0.038 | 1.30 | family with sequence similarity 171, member B |
| Stxbp5l | 0.002 | 0.015 | 1.29 | syntaxin binding protein 5-like |
| Bicd1 | 0.001 | 0.010 | 1.29 | bicaudal D homolog 1 (Drosophila) |
| Lrrcc1 | 0.005 | 0.045 | 1.28 | leucine rich repeat and coiled-coil domain containing 1 |
| Pbk | 0.001 | 0.011 | 1.28 | PDZ binding kinase |
| RGD1308139 | 0.004 | 0.035 | 1.26 | similar to RIKEN cDNA 1200014J11 |
| Mgat5b | 0.005 | 0.048 | 1.26 | mannosyl (alpha-1,6-)-glycoprotein B-1,6-N-acetyl-glucosaminyltransferase |
| Apaf1 | 0.003 | 0.025 | 1.25 | apoptotic peptidase activating factor 1 |
| Ppip5k1 | 0.005 | 0.043 | 1.24 | diphosphoinositol pentakisphosphate kinase 1 |
| Rfwd3 | 0.003 | 0.031 | 1.24 | ring finger and WD repeat domain 3 |
| Pcdhb20 | 0.002 | 0.020 | 1.23 | protocadherin beta 20 |
| LOC690326 | 0.004 | 0.033 | 1.23 | hypothetical protein LOC690326 |
| Morc3 | 0.001 | 0.008 | 1.23 | MORC family CW-type zinc finger 3 |
| Mab21l1 | 0.005 | 0.050 | 1.22 | mab-21-like 1 (C. elegans) |
| Nvl | 0.002 | 0.018 | 1.21 | nuclear VCP-like |
| LOC687082 | 0.005 | 0.047 | 1.21 | similar to olfactory receptor 508 |
| Senp5 | 0.004 | 0.041 | 1.20 | Sumo1/sentrin/SMT3 specific peptidase 5 |
| Gnaq | 0.001 | 0.013 | 1.20 | guanine nucleotide binding protein (G protein), q polypeptide |
| Rnf113a1 | 0.004 | 0.036 | 1.19 | ring finger protein 113A1 |
| Efna5 | 0.003 | 0.024 | 1.17 | ephrin A5 |
| Uhrf2 | 0.003 | 0.030 | 1.17 | ubiquitin-like with PHD and ring finger domains 2 |
| Ubn2 | 0.002 | 0.016 | 1.16 | ubinuclein 2 |
| Cenpk | 0.000 | 0.005 | 1.16 | centromere protein K |
| Zbtb44 | 0.004 | 0.034 | 1.15 | zinc finger and BTB domain containing 44 |
| Hoxa10 | 0.001 | 0.009 | 1.15 | homeo box A10 |
| Smc5 | 0.001 | 0.007 | 1.15 | structural maintenance of chromosomes 5 |
| LOC310487 | 0.004 | 0.042 | 1.14 | similar to purinergic receptor P2Y, G-protein coupled, 4 |
| Smarcad1 | 0.000 | 0.003 | 1.14 | SWI/SNF-related, matrix-associated actin-dependent regulator of chromatin |
| Tspan7 | 0.002 | 0.017 | 1.13 | tetraspanin 7 |
| Chd6 | 0.005 | 0.044 | 1.13 | chromodomain helicase DNA binding protein 6 |
| Cops3 | 0.003 | 0.026 | 1.11 | COP9 constitutive photomorphogenic homolog subunit 3 (Arabidopsis) |
| Chek1 | 0.004 | 0.040 | 1.11 | checkpoint kinase 1 |
| Sf3b1 | 0.003 | 0.023 | 1.10 | splicing factor 3b, subunit 1 |
| Stip1 | 0.003 | 0.027 | 1.09 | stress-induced phosphoprotein 1 |
| Rundc1 | 0.005 | 0.049 | 1.08 | RUN domain containing 1 |
| Thpo | 0.003 | 0.028 | 1.06 | thrombopoietin |
| The q-value was calculated using modified Benjamini-Hochberg. | | | | |

▶ **Table 2S** Top down-regulated genes in *Chl1*-silened cells vs. control.

| Gene Symbol | p-value | q-value | FC | Gene Name |
|---|---|---|---|---|
| Serpina6 | 0.003 | 0.027 | −3.02 | serpin peptidase inhibitor, clade A, member 6 |
| Emp1 | 0.004 | 0.034 | −1.95 | epithelial membrane protein 1 |
| Klk1 | 0.002 | 0.018 | −1.87 | kallikrein 1 |
| Rnf186 | 0.002 | 0.015 | −1.68 | ring finger protein 186 |
| Aqp5 | 0.005 | 0.048 | −1.62 | aquaporin 5 |
| Cd74 | 0.003 | 0.032 | −1.59 | Cd74 molecule, major histocompatibility complex, class II |
| Pcsk6 | 0.004 | 0.042 | −1.53 | proprotein convertase subtilisin/kexin type 6 |
| Gsn | 0.004 | 0.038 | −1.50 | gelsolin |
| Serpina1 | 0.004 | 0.039 | −1.48 | serpin peptidase inhibitor, clade A (α-1 antiproteinase, antitrypsin) |
| Olr782 | 0.005 | 0.049 | −1.42 | olfactory receptor 782 |
| Sdc1 | 0.003 | 0.025 | −1.42 | syndecan 1 |
| Chdh | 0.002 | 0.013 | −1.41 | choline dehydrogenase |
| Rasa4 | 0.001 | 0.010 | −1.39 | RAS p21 protein activator 4 |
| Bak1 | 0.001 | 0.005 | −1.38 | BCL2-antagonist/killer 1 |
| Prrg2 | 0.001 | 0.011 | −1.38 | proline rich Gla (G-carboxyglutamic acid) 2 |
| Cpne2 | 0.003 | 0.030 | −1.38 | copine II |
| PVR | 0.004 | 0.035 | −1.37 | poliovirus receptor |
| Reep6 | 0.004 | 0.046 | −1.35 | receptor accessory protein 6 |
| Cib1 | 0.002 | 0.023 | −1.35 | calcium and integrin binding 1 (calmyrin) |
| Pdzrn4 | 0.002 | 0.021 | −1.34 | PDZ domain containing RING finger 4 |
| Apobec4 | 0.000 | 0.004 | −1.34 | apolipoprotein B mRNA editing enzyme, catalytic polypeptide-like 4 |
| Foxa1 | 0.004 | 0.043 | −1.34 | forkhead box A1 |
| B4galt6 | 0.000 | 0.002 | −1.31 | UDP-Gal:betaGlcNAc beta 1,4-galactosyltransferase, polypeptide 6 |
| Fbxo2 | 0.001 | 0.013 | −1.30 | F-box protein 2 |
| Vsig10l | 0.003 | 0.029 | −1.28 | V-set and immunoglobulin domain containing 10 like |
| B3gnt3 | 0.002 | 0.014 | −1.28 | UDP-GlcNAc:betaGal beta-1,3-N-acetylglucosaminyltransferase 3 |
| Pdia2 | 0.004 | 0.036 | −1.28 | protein disulfide isomerase family A, member 2 |
| Dnajc22 | 0.000 | 0.003 | −1.28 | DnaJ (Hsp40) homolog, subfamily C, member 22 |
| Cat | 0.004 | 0.037 | −1.27 | catalase |
| Xrcc5 | 0.000 | 0.001 | −1.27 | X-ray repair complementing defective repair in Chinese hamster cells |
| Ninj1 | 0.001 | 0.008 | −1.26 | ninjurin 1 |
| Cdc14a | 0.004 | 0.040 | −1.26 | CDC14 cell division cycle 14 homolog A (S. cerevisiae) |
| Slc50a1 | 0.004 | 0.044 | −1.24 | solute carrier family 50 (sugar transporter), member 1 |
| RGD1566029 | 0.003 | 0.026 | −1.24 | similar to mKIAA1644 protein |
| Ppp1r3b | 0.005 | 0.046 | −1.23 | protein phosphatase 1, regulatory subunit 3B |
| Tesk1 | 0.004 | 0.038 | −1.22 | testis-specific kinase 1 |
| Casq1 | 0.002 | 0.021 | −1.22 | calsequestrin 1 (fast-twitch, skeletal muscle) |
| RGD1563547 | 0.002 | 0.022 | −1.21 | RGD1563547 |
| Isyna1 | 0.001 | 0.007 | −1.21 | inositol-3-phosphate synthase 1 |
| Mpzl3 | 0.005 | 0.047 | −1.21 | myelin protein zero-like 3 |
| Slc35a4 | 0.001 | 0.006 | −1.20 | solute carrier family 35, member A4 |
| Pik3r5 | 0.002 | 0.016 | −1.20 | phosphoinositide-3-kinase, regulatory subunit 5 |
| Itfg3 | 0.003 | 0.031 | −1.18 | integrin alpha FG-GAP repeat containing 3 |
| Olr68 | 0.001 | 0.009 | −1.17 | olfactory receptor 68 |
| Slc35e3 | 0.002 | 0.017 | −1.17 | solute carrier family 35, member E3 |
| Napa | 0.004 | 0.045 | −1.15 | N-ethylmaleimide-sensitive factor attachment protein, alpha |
| Cdk2ap1 | 0.004 | 0.033 | −1.15 | cyclin-dependent kinase 2 associated protein 1 |
| Dgkz | 0.002 | 0.019 | −1.14 | diacylglycerol kinase zeta |
| St8sia3 | 0.004 | 0.041 | −1.14 | ST8 alpha-N-acetyl-neuraminide alpha-2,8-sialyltransferase 3 |
| Scn9a | 0.002 | 0.024 | −1.12 | sodium channel, voltage-gated, type IX, alpha |
| Clic1 | 0.002 | 0.020 | −1.10 | chloride intracellular channel 1 |

▶ **Table 2S** Continued.

| Gene Symbol | p-value | q-value | FC | Gene Name |
|---|---|---|---|---|
| Mid1ip1 | 0.003 | 0.028 | −1.09 | MID1 interacting protein 1 (gastrulation specific G12 homolog |
| Atp12a | 0.000 | 0.004 | −1.08 | ATPase, H + / K + transporting, nongastric, alpha polypeptide |
| Wbscr17 | 0.003 | 0.029 | −1.08 | Williams-Beuren syndrome chromosome region 17 homolog |
| RGD1311343 | 0.005 | 0.050 | −1.08 | similar to RIKEN cDNA 4930524B15 |
| Stard7 | 0.001 | 0.012 | −1.06 | StAR-related lipid transfer (START) domain containing 7 |

The q-value was calculated using modified Benjamini-Hochberg.

▶ **Table 3S** List of pathways with significant enrichment between *Chl1* silenced cells or controls.

| Pathway | SIZE | ES (enrichment score) | NES (Normalized enrichment score) | NOM p-val | FDR q-val |
|---|---|---|---|---|---|
| REACTOME_SIGNALLING_TO_RAS | 18 | 0.53059 | 1.5473 | 0 | 0.087678 |
| REACTOME_SIGNALLING_TO_ERKS | 20 | 0.52248 | 1.8166 | 0 | 0.025661 |
| REACTOME_POST_TRANSLATIONAL_PROTEIN_MODIFICATION | 129 | 0.43992 | 1.5242 | 0 | 0.0943 |
| KEGG_TIGHT_JUNCTION | 78 | 0.37725 | 1.4817 | 0 | 0.10347 |
| KEGG_FOCAL_ADHESION | 128 | 0.44428 | 1.4643 | 0 | 0.11193 |
| GO_CELL_CYCLE_G1_S_PHASE_TRANSITION | 61 | 0.42192 | 1.6747 | 0 | 0.088851 |
| BIOCARTA_KERATINOCYTE_PATHWAY | 35 | 0.46716 | 1.7625 | 0 | 0.039862 |
| PID_ALPHA_SYNUCLEIN_PATHWAY | 23 | 0.61159 | 1.5292 | 0 | 0.093404 |
| GO_POSITIVE_REGULATION_OF_ENDOCYTOSIS | 79 | 0.56052 | 1.8715 | 0 | 0.062322 |
| PID_P73PATHWAY | 48 | 0.41707 | 1.5513 | 0 | 0.087718 |
| KEGG_B_CELL_RECEPTOR_SIGNALING_PATHWAY | 43 | 0.51313 | 1.6488 | 0 | 0.062241 |
| KEGG_SMALL_CELL_LUNG_CANCER | 52 | 0.47362 | 1.511 | 0 | 0.096805 |
| KEGG_APOPTOSIS | 63 | 0.49417 | 1.5686 | 0 | 0.086171 |
| GO_REGULATION_OF_STEROID_HORMONE_SECRETION | 18 | 0.59047 | 1.5645 | 0 | 0.11029 |
| BIOCARTA_GH_PATHWAY | 18 | 0.48423 | 1.5585 | 0 | 0.088921 |
| PID_TXA2PATHWAY | 42 | 0.37629 | 1.3255 | 0 | 0.18466 |
| KEGG_T_CELL_RECEPTOR_SIGNALING_PATHWAY | 71 | 0.44692 | 1.5287 | 0 | 0.09335 |
| PID_TRKR_PATHWAY | 30 | 0.48806 | 1.5694 | 0 | 0.086542 |
| GO_CHROMATIN_SILENCING | 25 | 0.38752 | 1.572 | 0 | 0.10735 |
| PID_CASPASE_PATHWAY | 40 | 0.50076 | 1.4395 | 0 | 0.12341 |
| GSE1432_1H_VS_24H_IFNG_MICROGLIA_UP | 132 | 0.447 | 1.626 | 0 | 0.017671 |
| GSE11924_TH2_VS_TH17_CD4_TCELL_UP | 134 | 0.41128 | 1.606 | 0 | 0.01901 |
| KEGG_MTOR_SIGNALING_PATHWAY | 33 | 0.32517 | 1.4478 | 0 | 0.11843 |
| PID_HIV_NEF_PATHWAY | 28 | 0.52236 | 1.5489 | 0 | 0.087383 |
| GSE1432_1H_VS_6H_IFNG_MICROGLIA_DN | 115 | 0.43142 | 1.3544 | 0 | 0.067894 |
| GSE12845_IGD_POS_VS_NEG_BLOOD_BCELL_UP | 115 | 0.40606 | 1.6149 | 0 | 0.0184 |
| REACTOME_CELL_CELL_COMMUNICATION | 86 | 0.40803 | 1.3949 | 0 | 0.14804 |
| GSE11057_NAIVE_VS_MEMORY_CD4_TCELL_DN | 123 | 0.37524 | 1.3571 | 0 | 0.066383 |
| GSE13411_IGM_VS_SWITCHED_MEMORY_BCELL_UP | 137 | 0.40862 | 1.4873 | 0 | 0.032303 |
| GSE1460_CD4_THYMOCYTE_VS_NAIVE_CD4_TCELL_ADULT_BLOOD_DN | 122 | 0.49469 | 1.6596 | 0 | 0.016118 |
| PID_ERBB1_INTERNALIZATION_PATHWAY | 20 | 0.41443 | 1.4887 | 0 | 0.10014 |
| PID_P53_DOWNSTREAM_PATHWAY | 85 | 0.44262 | 1.4974 | 0 | 0.099347 |
| KEGG_GALACTOSE_METABOLISM | 18 | 0.42745 | 1.4679 | 0 | 0.11079 |
| GSE13306_RA_VS_UNTREATED_MEM_CD4_TCELL_DN | 132 | 0.42874 | 1.4366 | 0 | 0.041245 |
| GSE10325_CD4_TCELL_VS_BCELL_DN | 129 | 0.38576 | 1.5807 | 0 | 0.022091 |
| PID_FCER1_PATHWAY | 42 | 0.46422 | 1.7126 | 0 | 0.047768 |
| PID_PTP1B_PATHWAY | 33 | 0.47609 | 1.466 | 0 | 0.11186 |
| KEGG_ECM_RECEPTOR_INTERACTION | 60 | 0.52691 | 1.4982 | 0 | 0.098039 |

| Pathway | SIZE | ES (enrich-ment score) | NES (Normalized enrichment score) | NOM p-val | FDR q-val |
|---|---|---|---|---|---|
| GSE11057_CD4_EFF_MEM_VS_PBMC_DN | 127 | 0.44815 | 1.3722 | 0 | 0.060606 |
| PID_INTEGRIN3_PATHWAY | 28 | 0.52963 | 1.6645 | 0 | 0.0639 |
| GO_RECEPTOR_INTERNALIZATION | 39 | 0.60076 | 1.6642 | 0 | 0.090233 |
| KEGG_CHRONIC_MYELOID_LEUKEMIA | 40 | 0.45325 | 1.465 | 0 | 0.11182 |
| GSE10325_CD4_TCELL_VS_MYELOID_DN | 152 | 0.38608 | 1.5025 | 0 | 0.030464 |
| KEGG_INOSITOL_PHOSPHATE_METABOLISM | 37 | 0.46707 | 1.3713 | 0 | 0.16059 |
| GO_GROWTH_FACTOR_BINDING | 95 | 0.49337 | 1.6102 | 0 | 0.10802 |
| REACTOME_TRANSPORT_OF_GLUCOSE_AND_OTHER_SUGARS_BILE_SALTS_AND_ORGANIC_ACIDS_METAL_IONS_AND_AMINE_COMPOUNDS | 73 | 0.4827 | 1.4831 | 0 | 0.10223 |
| GO_RECEPTOR_METABOLIC_PROCESS | 57 | 0.49738 | 1.4184 | 0 | 0.15435 |
| ST_TUMOR_NECROSIS_FACTOR_PATHWAY | 23 | 0.55075 | 1.6449 | 0 | 0.063119 |
| GSE14000_UNSTIM_VS_4H_LPS_DC_DN | 132 | 0.44348 | 1.4877 | 0 | 0.032323 |
| KEGG_TOLL_LIKE_RECEPTOR_SIGNALING_PATHWAY | 62 | 0.39635 | 1.386 | 0 | 0.15317 |
| GSE14769_UNSTIM_VS_20MIN_LPS_BMDM_DN | 123 | 0.4278 | 1.5208 | 0 | 0.026845 |
| REACTOME_SIGNALING_BY_ERBB2 | 65 | 0.35559 | 1.3898 | 0 | 0.15003 |
| PID_RETINOIC_ACID_PATHWAY | 21 | 0.47785 | 1.5214 | 0 | 0.095577 |
| GSE14350_IL2RB_KO_VS_WT_TREG_DN | 138 | 0.36883 | 1.4609 | 0 | 0.035916 |
| GSE11057_NAIVE_VS_MEMORY_CD4_TCELL_UP | 103 | 0.43014 | 1.6844 | 0 | 0.014308 |
| BIOCARTA_BCR_PATHWAY | 22 | 0.53371 | 1.4376 | 0 | 0.12425 |
| GO_POSITIVE_REGULATION_OF_SMALL_GTPASE_MEDIATED_SIGNAL_TRANSDUCTION | 29 | 0.55435 | 1.5272 | 0 | 0.12571 |
| GSE13306_TREG_VS_TCONV_LAMINA_PROPRIA_UP | 136 | 0.38335 | 1.4678 | 0 | 0.034662 |
| GSE14308_NAIVE_CD4_TCELL_VS_INDUCED_TREG_DN | 117 | 0.33884 | 1.5169 | 0 | 0.027297 |
| GO_NEGATIVE_REGULATION_OF_SMALL_GTPASE_MEDIATED_SIGNAL_TRANSDUCTION | 24 | 0.5386 | 1.5973 | 0 | 0.10679 |
| GSE13411_SWITCHED_MEMORY_BCELL_VS_PLASMA_CELL_DN | 134 | 0.37454 | 1.3036 | 0 | 0.091443 |
| GSE13306_TREG_VS_TCONV_UP | 137 | 0.37909 | 1.467 | 0 | 0.034839 |
| GSE13484_UNSTIM_VS_3H_YF17D_VACCINE_STIM_PBMC_DN | 125 | 0.34663 | 1.4357 | 0 | 0.041458 |
| GSE13484_12H_VS_3H_YF17D_VACCINE_STIM_PBMC_DN | 120 | 0.3489 | 1.4231 | 0 | 0.043712 |
| GSE11057_NAIVE_VS_CENT_MEMORY_CD4_TCELL_DN | 115 | 0.35098 | 1.4124 | 0 | 0.047033 |
| GSE10325_BCELL_VS_MYELOID_UP | 119 | 0.39192 | 1.4972 | 0 | 0.030904 |
| GSE14308_TH2_VS_TH17_UP | 114 | 0.39971 | 1.7439 | 0 | 0.012961 |
| GSE11057_NAIVE_CD4_VS_PBMC_CD4_TCELL_UP | 110 | 0.4165 | 1.6644 | 0 | 0.014964 |
| KAECH_NAIVE_VS_MEMORY_CD8_TCELL_UP | 112 | 0.37807 | 1.6917 | 0 | 0.013427 |
| GSE12845_IGD_POS_BLOOD_VS_PRE_GC_TONSIL_BCELL_UP | 107 | 0.37828 | 1.7194 | 0 | 0.011744 |
| GSE10325_BCELL_VS_LUPUS_BCELL_DN | 133 | 0.4154 | 1.3 | 0 | 0.093637 |
| GO_NEGATIVE_REGULATION_OF_CELLULAR_RESPONSE_TO_GROWTH_FACTOR_STIMULUS | 78 | 0.4232 | 1.4137 | 0 | 0.15555 |
| KEGG_REGULATION_OF_ACTIN_CYTOSKELETON | 139 | 0.37403 | 1.4425 | 0 | 0.12151 |
| GO_NEGATIVE_REGULATION_OF_GENE_EXPRESSION_EPIGENETIC | 36 | 0.4136 | 1.8416 | 0 | 0.052075 |
| KEGG_ERBB_SIGNALING_PATHWAY | 52 | 0.42031 | 1.5627 | 0 | 0.086275 |
| GSE15324_ELF4_KO_VS_WT_NAIVE_CD8_TCELL_UP | 133 | 0.34889 | 1.6598 | 0 | 0.01604 |
| REACTOME_APOPTOTIC_CLEAVAGE_OF_CELLULAR_PROTEINS | 26 | 0.44783 | 1.7642 | 0 | 0.039997 |
| KEGG_MAPK_SIGNALING_PATHWAY | 193 | 0.38847 | 1.5256 | 0 | 0.093546 |
| PID_HDAC_CLASSII_PATHWAY | 15 | 0.55341 | 1.5566 | 0 | 0.087862 |
| BIOCARTA_IL2RB_PATHWAY | 25 | 0.47913 | 1.3771 | 0 | 0.15704 |
| GOLDRATH_NAIVE_VS_MEMORY_CD8_TCELL_DN | 144 | 0.43163 | 1.3677 | 0 | 0.061839 |
| GSE15659_CD45RA_NEG_CD4_TCELL_VS_ACTIVATED_TREG_UP | 112 | 0.38956 | 1.3737 | 0 | 0.060005 |
| KEGG_CHEMOKINE_SIGNALING_PATHWAY | 122 | 0.41455 | 1.4543 | 0 | 0.11534 |
| GO_OLIGODENDROCYTE_DEVELOPMENT | 24 | 0.54677 | 1.5199 | 0 | 0.12744 |

▶ **Table 3S** Continued.

| Pathway | SIZE | ES (enrichment score) | NES (Normalized enrichment score) | NOM p-val | FDR q-val |
|---|---|---|---|---|---|
| GSE13485_DAY7_VS_DAY21_YF17D_VACCINE_PBMC_UP | 114 | 0.37314 | 1.4143 | 0 | 0.045893 |
| KEGG_AXON_GUIDANCE | 86 | 0.52622 | 1.5698 | 0 | 0.08668 |
| BIOCARTA_IL6_PATHWAY | 17 | 0.57366 | 1.7064 | 0 | 0.051554 |
| PID_MAPK_TRK_PATHWAY | 24 | 0.50601 | 1.513 | 0 | 0.096274 |
| REACTOME_DOWNSTREAM_SIGNALING_EVENTS_OF_B_CELL_RECEPTOR_BCR | 53 | 0.33299 | 1.3988 | 0 | 0.14684 |
| PID_IL2_STAT5_PATHWAY | 21 | 0.52689 | 1.3376 | 0 | 0.17916 |
| GSE14769_UNSTIM_VS_120MIN_LPS_BMDM_DN | 144 | 0.405 | 1.4506 | 0 | 0.037751 |
| GSE14000_4H_VS_16H_LPS_DC_TRANSLATED_RNA_UP | 143 | 0.38932 | 1.4448 | 0 | 0.039465 |
| GSE13738_RESTING_VS_TCR_ACTIVATED_CD4_TCELL_DN | 117 | 0.35432 | 1.5391 | 0 | 0.024861 |
| GSE14000_UNSTIM_VS_16H_LPS_DC_TRANSLATED_RNA_DN | 109 | 0.40485 | 1.3948 | 0 | 0.053315 |
| REACTOME_METABOLISM_OF_LIPIDS_AND_LIPOPROTEINS | 320 | 0.36353 | 1.3562 | 0 | 0.16946 |
| GSE13485_PRE_VS_POST_YF17D_VACCINATION_PBMC_DN | 126 | 0.39151 | 1.336 | 0 | 0.074941 |
| REACTOME_TRIF_MEDIATED_TLR3_SIGNALING | 51 | 0.37108 | 1.3648 | 0 | 0.16467 |
| REACTOME_CELL_SURFACE_INTERACTIONS_AT_THE_VASCULAR_WALL | 60 | 0.54008 | 1.5914 | 0 | 0.082887 |
| KEGG_INSULIN_SIGNALING_PATHWAY | 91 | 0.38395 | 1.7156 | 0 | 0.048743 |
| GSE15659_RESTING_TREG_VS_NONSUPPRESSIVE_TCELL_UP | 104 | 0.39343 | 1.4214 | 0 | 0.044049 |
| PID_P75_NTR_PATHWAY | 47 | 0.41386 | 1.4279 | 0 | 0.12659 |
| GSE14000_UNSTIM_VS_16H_LPS_DC_DN | 122 | 0.40683 | 1.371 | 0 | 0.06106 |
| GSE13485_CTRL_VS_DAY3_YF17D_VACCINE_PBMC_DN | 120 | 0.38902 | 1.3844 | 0 | 0.056173 |
| GSE10325_BCELL_VS_MYELOID_DN | 144 | 0.40524 | 1.4295 | 0 | 0.042364 |
| GSE14308_TH2_VS_TH1_DN | 125 | 0.34869 | 1.5618 | 0 | 0.022855 |
| GSE14350_IL2RB_KO_VS_WT_TEFF_UP | 124 | 0.38755 | 1.5648 | 0 | 0.0221 |
| GSE1460_CD4_THYMOCYTE_VS_NAIVE_CD4_TCELL_CORD_BLOOD_DN | 121 | 0.37638 | 1.5572 | 0 | 0.023362 |
| GSE14769_UNSTIM_VS_60MIN_LPS_BMDM_DN | 137 | 0.34295 | 1.3892 | 0 | 0.054589 |
| BIOCARTA_COMP_PATHWAY | 15 | 0.56406 | 1.4016 | 0 | 0.1454 |
| GSE13485_DAY3_VS_DAY7_YF17D_VACCINE_PBMC_DN | 125 | 0.44325 | 1.6254 | 0 | 0.017783 |
| GSE15659_CD45RA_NEG_CD4_TCELL_VS_NONSUPPRESSIVE_TCELL_UP | 112 | 0.4736 | 1.7683 | 0 | 0.012037 |
| GSE10325_LUPUS_CD4_TCELL_VS_LUPUS_BCELL_DN | 131 | 0.36483 | 1.3863 | 0 | 0.055731 |
| PID_CD40_PATHWAY | 22 | 0.50086 | 1.7626 | 0 | 0.040408 |
| GSE13229_IMM_VS_MATURE_NKCELL_DN | 118 | 0.42681 | 1.7205 | 0 | 0.011908 |
| GSE13306_TREG_VS_TCONV_SPLEEN_UP | 132 | 0.45153 | 1.545 | 0 | 0.023932 |
| GSE13738_TCR_VS_BYSTANDER_ACTIVATED_CD4_TCELL_DN | 128 | 0.46931 | 1.8208 | 0 | 0.008238 |
| SIG_CD40PATHWAYMAP | 22 | 0.42431 | 1.4123 | 0 | 0.13778 |
| GSE11864_CSF1_VS_CSF1_IFNG_IN_MAC_UP | 106 | 0.35991 | 1.3688 | 0 | 0.061674 |
| GSE10325_MYELOID_VS_LUPUS_MYELOID_DN | 128 | 0.44294 | 1.4182 | 0 | 0.045185 |
| KEGG_NEUROTROPHIN_SIGNALING_PATHWAY | 69 | 0.40381 | 1.4644 | 0 | 0.11206 |
| GSE14308_TH1_VS_TH17_UP | 124 | 0.39875 | 1.7039 | 0 | 0.013281 |
| PID_TCR_PATHWAY | 48 | 0.4097 | 1.3817 | 0 | 0.15559 |
| GSE1460_CD4_THYMOCYTE_VS_THYMIC_STROMAL_CELL_DN | 125 | 0.4132 | 1.5912 | 0 | 0.02098 |
| GSE14000_UNSTIM_VS_4H_LPS_DC_TRANSLATED_RNA_DN | 128 | 0.4474 | 1.367 | 0 | 0.062089 |
| GSE11057_NAIVE_VS_EFF_MEMORY_CD4_TCELL_UP | 112 | 0.41766 | 1.5163 | 0 | 0.027392 |
| GSE1448_CTRL_VS_ANTI_VALPHA2_DP_THYMOCYTE_UP | 129 | 0.34507 | 1.4934 | 0 | 0.031805 |
| KEGG_GLIOMA | 39 | 0.45128 | 1.5989 | 0 | 0.081749 |
| GSE13738_TCR_VS_BYSTANDER_ACTIVATED_CD4_TCELL_UP | 119 | 0.49569 | 1.8364 | 0 | 0.006533 |
| KEGG_NATURAL_KILLER_CELL_MEDIATED_CYTOTOXICITY | 65 | 0.46141 | 1.4229 | 0 | 0.12964 |
| KEGG_RETINOL_METABOLISM | 33 | 0.5528 | 1.4062 | 0 | 0.14176 |

| Pathway | SIZE | ES (enrich-ment score) | NES (Normalized enrichment score) | NOM p-val | FDR q-val |
|---|---|---|---|---|---|
| GO_14_3_3_PROTEIN_BINDING | 15 | 0.6012 | 1.4718 | 0 | 0.13943 |
| GO_POSITIVE_REGULATION_OF_LYMPHOCYTE_MIGRATION | 22 | 0.65228 | 1.5994 | 0 | 0.10965 |
| GSE11057_EFF_MEM_VS_CENT_MEM_CD4_TCELL_UP | 131 | 0.37899 | 1.5885 | 0 | 0.021558 |
| KAECH_DAY15_EFF_VS_MEMORY_CD8_TCELL_UP | 134 | 0.43136 | 1.586 | 0 | 0.021861 |
| GO_MUCOPOLYSACCHARIDE_METABOLIC_PROCESS | 81 | 0.45731 | 1.4807 | 0 | 0.13632 |
| GO_GLYCOPROTEIN_METABOLIC_PROCESS | 243 | 0.41041 | 1.5547 | 0 | 0.11286 |
| GO_PHOSPHATIDYLCHOLINE_BIOSYNTHETIC_PROCESS | 20 | 0.5341 | 1.586 | 0 | 0.10598 |
| GO_CHAPERONE_MEDIATED_PROTEIN_FOLDING | 32 | 0.48073 | 1.6097 | 0 | 0.10852 |
| KEGG_VEGF_SIGNALING_PATHWAY | 45 | 0.41948 | 1.4046 | 0 | 0.14285 |
| GO_DISULFIDE_OXIDOREDUCTASE_ACTIVITY | 22 | 0.46034 | 1.5175 | 0 | 0.12682 |
| GO_POSITIVE_REGULATION_OF_SEQUENCE_SPECIFIC_DNA_BIND-ING_TRANSCRIPTION_FACTOR_ACTIVITY | 156 | 0.40489 | 1.4156 | 0 | 0.15544 |
| GO_SH3_DOMAIN_BINDING | 76 | 0.38087 | 1.5578 | 0 | 0.11204 |
| GO_ANGIOGENESIS | 220 | 0.47305 | 1.4983 | 0 | 0.13042 |
| GSE11057_NAIVE_VS_EFF_MEMORY_CD4_TCELL_DN | 128 | 0.3686 | 1.4566 | 0 | 0.036455 |
| REACTOME_DOWNSTREAM_SIGNAL_TRANSDUCTION | 58 | 0.34978 | 1.3589 | 0 | 0.16791 |
| REACTOME_DEVELOPMENTAL_BIOLOGY | 239 | 0.34249 | 1.4482 | 0 | 0.1184 |
| GO_RESPONSE_TO_IRON_ION | 29 | 0.51758 | 1.6858 | 0 | 0.085366 |
| GO_LIPID_HOMEOSTASIS | 77 | 0.46214 | 1.4636 | 0 | 0.14178 |
| GO_ATP_DEPENDENT_CHROMATIN_REMODELING | 23 | 0.43978 | 1.5494 | 0 | 0.11662 |
| GO_REPRESSING_TRANSCRIPTION_FACTOR_BINDING | 23 | 0.40559 | 1.699 | 0 | 0.073468 |
| GO_CARBOHYDRATE_DERIVATIVE_CATABOLIC_PROCESS | 122 | 0.39143 | 1.4351 | 0 | 0.14875 |
| GO_GASTRULATION_WITH_MOUTH_FORMING_SECOND | 20 | 0.57747 | 1.4943 | 0 | 0.13198 |
| GO_FIBRINOLYSIS | 18 | 0.6206 | 1.5127 | 0 | 0.12943 |
| GO_HISTONE_EXCHANGE | 19 | 0.45138 | 1.4891 | 0 | 0.13253 |
| GO_POSITIVE_REGULATION_OF_WOUND_HEALING | 34 | 0.52132 | 1.6829 | 0 | 0.087992 |
| GO_AMINOGLYCAN_METABOLIC_PROCESS | 124 | 0.43434 | 1.4583 | 0 | 0.14387 |
| GO_INSULIN_LIKE_GROWTH_FACTOR_BINDING | 23 | 0.56556 | 1.5934 | 0 | 0.10598 |
| GO_NEGATIVE_REGULATION_OF_PEPTIDYL_SERINE_PHOSPHO-RYLATION | 15 | 0.57413 | 1.5758 | 0 | 0.1068 |
| GO_ACTIN_CYTOSKELETON_REORGANIZATION | 36 | 0.54668 | 1.5851 | 0 | 0.10645 |
| GO_REGULATION_OF_WOUND_HEALING | 99 | 0.49396 | 1.6493 | 0 | 0.10315 |
| GO_CELL_DIVISION | 233 | 0.33263 | 1.5974 | 0 | 0.1072 |
| GO_REGULATION_OF_MICROTUBULE_BASED_PROCESS | 131 | 0.37816 | 1.6844 | 0 | 0.086891 |
| GO_PHOTOTRANSDUCTION_VISIBLE_LIGHT | 15 | 0.58684 | 1.4473 | 0 | 0.14769 |
| GO_MYOBLAST_FUSION | 17 | 0.56552 | 1.7543 | 0 | 0.058993 |
| GO_CHROMATIN_ORGANIZATION | 285 | 0.28902 | 1.4617 | 0 | 0.14241 |
| GO_SINGLE_STRANDED_RNA_BINDING | 30 | 0.4138 | 1.5166 | 0 | 0.12691 |
| GO_REGULATION_OF_CENTROSOME_CYCLE | 20 | 0.44799 | 1.474 | 0 | 0.13945 |
| GO_TRANSFERASE_ACTIVITY_TRANSFERRING_PENTOSYL_GROUPS | 35 | 0.50719 | 1.8604 | 0 | 0.06453 |
| GO_DNA_PACKAGING | 74 | 0.31863 | 1.3085 | 0 | 0.20368 |
| GO_REGULATION_OF_INTRACELLULAR_STEROID_HORMONE_RE-CEPTOR_SIGNALING_PATHWAY | 31 | 0.37336 | 1.6135 | 0 | 0.10967 |
| GO_NEGATIVE_REGULATION_OF_INTRACELLULAR_STEROID_HORMONE_RECEPTOR_SIGNALING_PATHWAY | 17 | 0.41655 | 1.5724 | 0 | 0.10711 |
| GO_CHROMATIN_ASSEMBLY_OR_DISASSEMBLY | 63 | 0.37804 | 1.5148 | 0 | 0.12732 |
| GO_REGULATION_OF_B_CELL_DIFFERENTIATION | 18 | 0.54486 | 1.6691 | 0 | 0.087947 |
| GO_CELLULAR_RESPONSE_TO_IONIZING_RADIATION | 27 | 0.39111 | 1.5356 | 0 | 0.12206 |